

Full Wave Modeling of Brain Waves as Electromagnetic Waves

Sidharath Jain¹, *, Raj Mittra¹, and Joe Wiart²

(Invited Paper)

Abstract—This paper describes a novel technique which has the potential to make a significant impact on the mapping of the human brain. This technique has been designed for 3D full-wave electromagnetic simulation of waves at very low frequencies and has been applied to the problem of modeling of brain waves which can be modeled as electromagnetic waves lying in the frequency range of 0.1–100 Hz. The use of this technique to model the brain waves inside the head enables one to solve the problem on a regular PC within 24 hrs, and requires just 1 GB of memory, as opposed to a few years of run time and nearly 200 Terabyte (200,000 GB) needed by the conventional FDTD (Finite Difference Time Domain) methods. The proposed technique is based on scaling the material parameters inside the head and solving the problem at a higher frequency (few tens of MHz) and then obtaining the actual fields at the frequency of interest (0.1–100 Hz) by using the fields computed at the higher frequency. The technique has been validated analytically by using the Mie Series solution for a homogeneous sphere, as well as numerically for a sphere, a finite lossy dielectric slab and the human head using the conventional Finite Difference Time Domain (FDTD) Method. The presented technique is universal and can be used to obtain full-wave solution to low-frequency problems in electromagnetics by using any numerical technique.

1. INTRODUCTION

Neural activity inside the brain results in low frequency waves known as brain waves. These brain waves can be further classified into delta (0.1 to 3 Hz), theta (4 to 7 Hz), alpha (8 to 12 Hz), beta (12 to 30 Hz) and gamma (30 to 100 Hz) waves based on the rate of neural activity inside the brain. For example the neural activity while sleeping can be modeled as alpha waves, while dreaming can be modeled as theta waves, when one is in a state of relaxation or conscious thinking or agitated state can be modeled as beta waves and when one is moving the limbs can be modeled as gamma waves. For the development of thought controlled devices one needs to focus on the mid-range beta (16–20 Hz) waves because when one is consciously thinking the neural activity can be modeled as electromagnetic waves in this frequency range. Researchers have succeeded in converting the brain wave patterns recorded by using electroencephalogram (EEG) into alphabets and words [1, 2]. Also, monitoring the brain waves can help diagnose disorders within the human body, and this possibility is currently being investigated by a number of researchers [3–6].

The Fast Fourier Transform (FFT) has been used to analyze the EEGs, in order to investigate the features of EEG signals in the frequency domain. As mentioned earlier, the frequency distribution of the EEG signal is highly correlated with the mental and emotional states of a person, as well as with the placement of the EEG electrodes. Commonly used EEG montages fall into two categories; namely,

Received 14 January 2015, Accepted 9 April 2015, Scheduled 1 May 2015

Invited paper for the Commemorative Collection on the 150-Year Anniversary of Maxwell's Equations.

* Corresponding author: Sidharath Jain (sidharathj@gmail.com).

¹ Electromagnetic Communication Laboratory, Department of Electrical Engineering, The Pennsylvania State University, University Park, PA 16802, USA. ² France Telecom R&D, France.

monopolar and bipolar [7]. The monopolar montages measure the signal at the point of contact and compare it with a common reference electrode which is placed in a location which is unaffected by brain activities. On the other hand, the bipolar montage only records the difference in the signals between two electrodes that are in contact with the scalp. Yet another area of brain research, carried out to harness the information from brain waves in the process of developing thought-controlled devices [8–11] is to develop dry electrodes that can provide the desired accuracy in brain wave measurements, since the traditional electrodes used for EEG measurements require a gel-based material to ensure good contact between the scalp and the electrodes [12, 13].

Although the EEG signals can be measured externally, it is not possible to determine the centers of neural activity inside the brain corresponding to different thoughts, and yet that is the key to converting one’s thoughts into actions as well as to diagnose and monitor the health problems. Full-wave electromagnetic modeling of brain waves has been proposed as a very promising alternative to overcome these challenges in mapping the human brain. However, it is well known that both the time domain and frequency domain based numerical computational electromagnetic methods for solving the Maxwell’s equations suffer from the so-called “low-frequency-breakdown” problem [14, 15]. It is not uncommon, therefore, to resort to quasi-static solvers once the frequency of interest falls below a certain frequency (say a few MHz), and to ignore the contribution of the displacement currents, and, hence, the coupling between the electric and magnetic fields. Specifically, the quasi-static solution assumes

Table 1. Material parameters of the 26 different materials present in the human head model in Figure 1 with their percentage contribution to the head model.

Material ID	Material Name	Percentage	Permittivity (Real)	Conductivity (S/m)	Permittivity (Im)
0	Air	71.6461	1.0	0	0.0
1	Internal air	0.6462	1.0	0	0.0
2	Body fluid	0.0546	99.0	1.5	−539781928.1
3	Eye-cornea	0.0013	1642100.0	0.4214	−151642736.3
4	Fat	5.6444	1472800.0	0.019555	−7036957.1
5	Lymph	0.0654	1637700.0	0.52142	−187635395.3
6	Mucous membrane	0.7369	51274.0	0.00042719	−153726.3
7	Nerve spine	0.0460	1608800.0	0.0274	−9860016.6
8	Muscle	5.6944	17719000.0	0.23329	−83950484.0
9	White matter	2.3688	5289800.0	0.053274	−19170895.0
10	Glands	0.3758	1637700.0	0.52142	−187635395.3
11	Blood vessel	0.0757	8095800.0	0.26115	−93976033.7
12	Cerebellum	0.6819	12108000.0	0.095258	−34279031.3
13	Cortical bone	1.7422	8867.8	0.020055	−7216884.4
14	Cartilage	0.1248	1637700.0	0.17143	−61689877.3
15	Ligament/Tendon	1.7546	17098000.0	0.26977	−97077980.5
16	Dry skin	2.5039	1136.0	0.0002	−71970.9
17	Tooth	0.0698	8867.8	0.020055	−7216884.4
18	Grey matter	2.7776	12107000.0	0.075258	−27081938.9
19	Eye lens	0.0048	1737200.0	0.32143	−115668070.1
20	Eye sclera	0.0176	292950.0	0.5027	−180898916.8
21	Blood	0.0489	5259.9	0.7	−251898233.1
22	Cerebrospinal fluid	0.8197	109.0	2	−719709237.5
23	Eye vitreous humor	0.0626	99.0	1.5	−539781928.1
24	Bonemarrow	0.6532	166680.0	0.0016487	−593292.3
25	Cancellous bone	1.3828	788910.0	0.080703	−29041347.3

that the real part of ε_r can be neglected since $\sigma/(\omega\varepsilon) \gg 1$ and transforms the wave equation into a diffusion equation. Unfortunately, however, this approximation is not valid for most of the materials inside the head, since the $\sigma/(\omega\varepsilon)$ ratio of these materials is typically close to 1 [16–21], as may be seen from Table 1. In fact, Grill et al. [22] have shown that the quasi-static potential differs from the full-wave potential by nearly 30% to 50%, supporting the argument that a full-wave solution should be derived even at low frequencies for the head-modeling problem, since the quasi-static approach is not sufficiently accurate for the problem at hand.

In this paper we propose a technique for deriving the full-wave solutions of the head problem at very low frequencies by first scaling the material parameters inside the head, then solving the problem at a higher frequency (few tens of MHz), and finally obtaining the actual fields at the frequency of interest (0.1–100 Hz) using the fields previously obtained at the higher frequency. The technique has been validated by comparing against the Mie-series analytical solution, as well as against the numerically-derived solution for a homogeneous lossy sphere. The solutions have also been validated for the case of a finite lossy dielectric slab, and for the human head, simulated by using the Finite Difference Time Domain (FDTD) Method. The technique proposed herein is universal, in that it can be used to obtain full-wave solution to low-frequency problems in electromagnetics by using any of the available CEM techniques and can be applied to solve most low-frequency problems as long as scaling the relative permittivity does not result in permittivity values much smaller than unity.

2. FULL-WAVE MODELING OF BRAIN WAVES

A model comprising of 26 different materials has been used to model the human head. This model has been discretized into voxels; i.e., cubes with side 1 mm. Figure 1 shows the material distribution inside the human head model along with two different cross-sections.

For the purpose of mapping the brain, we are interested in estimating the fields at different points inside the head in the frequency range of 0.1–100 Hz when a source is placed inside the head. However, placing a source inside the head is difficult to do, since the medium inside the head is lossy and highly dispersive, and ε_r for the different mediums range from nearly 10^2 to 10^8 , as may be seen from the material parameters for the human head at 50 Hz as listed in Table 1, where the imaginary part of the complex permittivity has been computed by using the relation $\text{Im}(\varepsilon_r) = -\sigma/(\omega\varepsilon_0)$. To circumvent this problem, we measure the field at different points inside the head with a short dipole source placed outside the head as the exciter. Alternatively, we could place the source inside the head, and sense the fields on the surface of the head, as for instance by using the Electro Encephalogram (EEG). We could invoke reciprocity to establish the equivalence between these two measurements, and then either measure or simulate the one that is most convenient for our purpose.

Figure 2 shows the cross-section of an adult human head, and also depicts a short dipole placed at three different locations on the head with different polarizations. The length of the dipole is 45 mm.

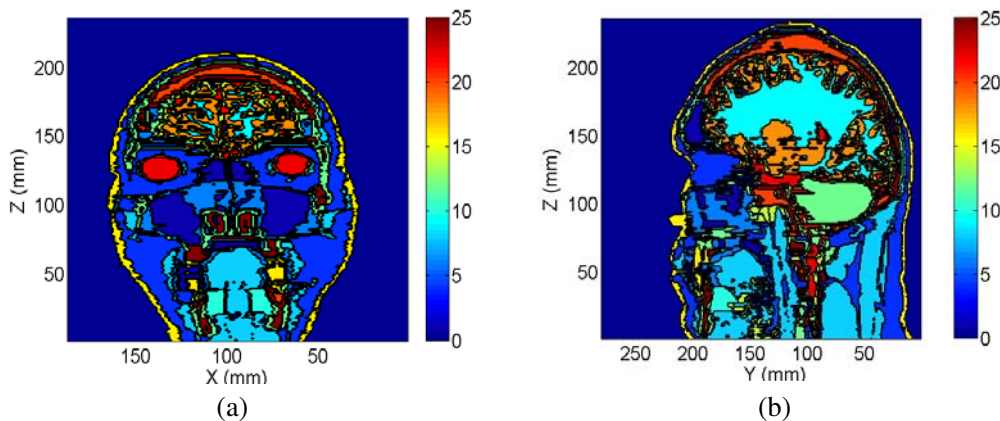


Figure 1. The material distribution inside the head model with 26 different materials for two perpendicular cross-sections of the head. (a) X - Z plane, (b) Y - Z plane.

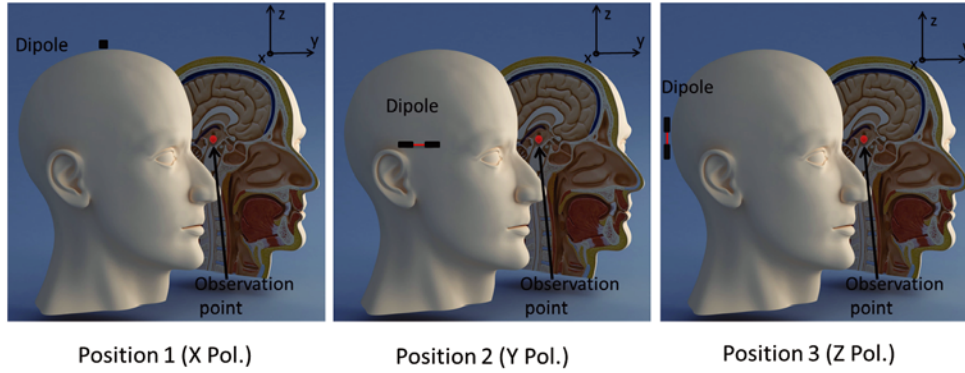


Figure 2. Human head model with three different orientations and locations of exciting short dipoles.

The material distribution inside the head is very complex (see Figure 1); hence, a very fine mesh ($\sim 1 \text{ mm} \times 1 \text{ mm} \times 1 \text{ mm}$) is needed to accurately model the head. As pointed out earlier, 3D electromagnetic solvers based on both the Method of Moments (MoM) and the Finite Element Method (FEM) suffer from the low-frequency breakdown problem, and they can only go down to a few hundred MHz in frequency, below which the result they yield becomes very inaccurate relatively quickly. Also, the number of unknowns required to solve the problem is estimated to be nearly 100 million, which requires exorbitantly high computational resources, both in terms of CPU memory and time. As has been pointed out earlier, we cannot use the quasi-static approximation to solve the problem at hand even though we are interested in the solution at very low frequencies, since the real and imaginary parts of the complex ε_{ri} are comparable to each other and, hence, the contribution of the displacement current cannot be neglected [22]. In view of this, we propose an alternative approach to derive the full-wave solution at such low frequencies, as explained below.

The Finite Difference Time Domain (FDTD) method appears to be best suited to solve the problem at hand. However, in the FDTD method a small mesh size implies a small time-step. In addition, if one is working at frequencies in the range of 0.1 Hz to 100 Hz, and is using a low-frequency Gaussian pulse for the excitation signal the small time-step would aggravate the problem even further, and one would need to wait for several hundred billion time-steps for the solution to converge. Also, at low frequencies, the Absorbing Boundary Conditions (ABCs) are not very effective, since they are not designed to absorb the evanescent part of the fields and hence, they have to be moved far away and the problem size would increase as a result. Thus, the conventional FDTD would be impractical to use for the head problem at frequencies of interest to us. Therefore, to overcome both of these problems, namely, long time domain pulses which lead to exorbitantly large simulation times and reflections from the ABC, we have developed a technique based on the scaling of the material parameters and solving the problem at a higher frequency — as shown in the schematic in Figure 3 — to derive the field values at the low frequencies we desire. The technique involves scaling the ε_{ri} of all the media inside the geometry to be analyzed according to the equation:

$$\varepsilon_{risc} = \varepsilon_{ri} \frac{f}{f_{sc}} \quad (1)$$

where ε_{risc} is the scaled ε_r of the medium with $\varepsilon_r = \varepsilon_{ri}$, f_{sc} the frequency at which the problem is actually solved, and f the frequency at which the solution is desired.

The effect of the scaling the ε_r of all the media according to Eq. (1) is that the ratio between the ε_r of two adjacent media remains constant, as a result of which the reflection and transmission coefficient at the interface between two semi-infinite media, which depends only on the ratio of the characteristic impedances of the two media remain unaltered. Also, if the medium thickness is much smaller than the wavelength, the effect of thickness on the reflection and transmission coefficient becomes negligible. Thus, the equivalent model of the head obtained by scaling the parameters of materials inside the head retains the values of the reflection and transmission coefficient between the material interfaces nearly same, because the size of the head is much smaller than the wavelength at the frequencies of interest; hence, the field distribution inside the head remains unchanged from the unscaled case. Also, since the

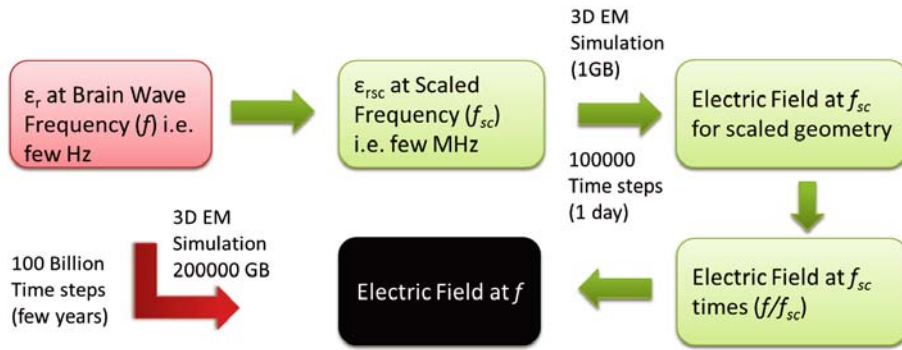


Figure 3. Schematic showing the steps involved in obtaining the full-wave solution at brain wave frequencies.

medium outside the head is free space, we do not scale the relative permittivity of free space as it would become much smaller than 1. To check the validity of this procedure we have shown, for the case of either a uniform sphere or a slab of lossy dielectric material, that by scaling the material parameters of the sphere/slab only, the electric field at a point inside the sphere or slab at the scaled frequency is also scaled by the same factor. It should be pointed out that the behavior of the magnetic field is dependent on the source, however, and the magnetic field inside the head remains nearly constant with scaling if the source is a plane wave. However, in common with the electric field, the value of the magnetic field also gets scaled by the same scaling factor if the source is a dipole. Also, we observe that since the skin depths in the low frequency range of interest here are very large compared to the dimension of the head. Hence, at low frequencies the head acts as a lossy cavity in which the waves bounce back and forth many times before they get attenuated completely.

The EEG can measure the brain waves, but these measurements do not lead to a unique solution to the inverse problem of locating the center of neural activity inside the brain. It is conjectured, however, that the development of techniques for efficient full-wave modeling of brain waves will not only open up avenues for addressing the problem of locating the center of neural activity, but would also enable us to correlate the different locations inside the brain with different thoughts and actions.

3. NUMERICAL RESULTS

3.1. Validation Using a Slab

To validate the proposed approach, we have considered the test case of a uniform lossy dielectric slab which is 300 mm long along both the transverse directions (x and y) and whose thickness is $D = 250$ mm, as shown in Figure 4. This value of the thickness was chosen because it is close to the size of head. For the material parameters, we choose $\epsilon_r = 10^7$, $\mu_r = 1$ and $\sigma = 0.01$ S/m at 1 Hz. Two different excitations were investigated. The first of these was an x -polarized dipole placed 10 mm above the slab as shown in Figure 4(a), while the second was an x -polarized plane wave incident from the top of the slab as shown in Figure 4(b). The dipole has a cross-section with side 5 mm and length equal to 45 mm including a gap of 5 mm between the two equal length arms. All references to the dipole excitation in this paper refer to a dipole with the above dimensions. For both of these cases, we observe the fields at a point located at the center of the slab.

Let us first consider the case of the dipole excitation. To solve this problem at $f = 1$ Hz, we need to run the conventional FDTD simulation of the original problem for several hundred billion time steps before it yields a convergent solution for the field. However, we can derive the same results in less than 10,000 time steps if we scale the ϵ_r of the slab by using the relation in Eq. (2) and work with a scaled frequency $f_{sc} = 50$ MHz. Table 2 shows that the amplitudes and phases of E_x and H_y at f remains virtually unchanged when we scale the frequency from 100 kHz to 50 MHz, modify the ϵ_r as mentioned above and scale the electric field and magnetic field values by the same factor f/f_{sc} , which was used to scale the ϵ_r to obtain the values of the fields at f . Furthermore, the number of time-steps required

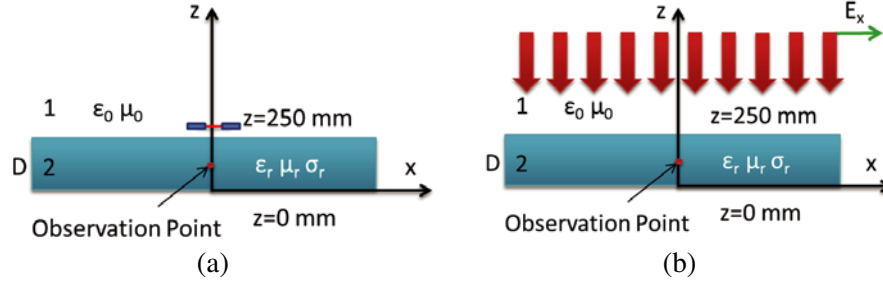


Figure 4. Infinite slab excited using a x -polarized. (a) Short dipole, (b) plane wave.

Table 2. The value of the x -component of the electric field and y -component of magnetic field at the center of the slab at 1 Hz due to an x -polarized short dipole as shown in Figure 4(a).

Frequency (fs) (MHz)	Ex		Hy		Time Steps
	Amp (nV/m)	Phase (rad)	Amp (pA/m)	Phase (rad)	
0.1	48.8	-1.6	37.7	2.0	400000
0.5	49.6	-1.6	32.4	1.6	60000
1	45.4	-1.6	29.8	1.6	16000
5	45.2	-1.7	29.6	1.5	11000
50	35.6	-2.2	27.9	1.3	8000

Table 3. The value of the x -component of the electric field and y -component of magnetic field at the center of the slab at 1 Hz due to an x -polarized plane wave incident on the slab as shown in Figure 4(b).

Frequency (fs) (MHz)	Ex		Hy		Time Steps
	Amp (nV/m)	Phase (rad)	Amp (nA/m)	Phase (rad)	
0.5	20.94	1.5	0.002654	3.1	16000
5	21.52	1.4	0.002655	3.1	6000

for convergence decreased from 400000 to 8000 as the solution frequency goes from 100 kHz to 50 MHz; i.e., a 50 times reduction in simulation time. For all of the cases investigated, the time signature of the field at the point where the field needs to be measured was plotted as a function of number of time steps. Furthermore, the time signature was processed, by using the Discrete Fourier Transform (DFT) at the frequency f_{sc} , as a function of the number of time steps (window indices), to demonstrate the convergence of the result at the frequency of interest and obtain the converged amplitude and phase of the fields at the measurement point.

For the case of a plane wave excitation (see Figure 4(b)), however, the value of the electric field at f_{sc} are scaled by the corresponding scaling factor but the value of the magnetic field at f_{sc} is same as that at f as listed in Table 3. This behavior of the electric field and the magnetic field for the dipole and plane wave excitations is found to hold true for any geometry as we will soon see. We point out that as long as $D/\lambda \ll 1$, the proposed scaling approach gives accurate solutions for the fields. We can accelerate the solution by several orders of magnitude by following the proposed scaling approach. It is also worthwhile to mention that if the scaled ε_r is < 1 , we can still use the proposed method, simply

by employing the Drude model, and expressing the complex ϵ_r as:

$$\epsilon_r = \epsilon_\infty - \frac{f_p^2}{f^2 - jf\gamma_p} \tag{2}$$

For a given frequency, the values of f_p and γ_p can be calculated to obtain the required value of ϵ_{rsc} at the frequency f of interest.

3.2. Validation Using a Sphere

Next, to validate our result for a problem which is analytically tractable, we consider a sphere whose radius is 120 mm (almost the size of the head), and which is filled with muscle tissue with material parameters $\epsilon_r = 17719000$, $\mu_r = 1$, $\sigma_r = 0.23329$ S/m at 50 Hz as shown in Figure 5(a). The analytical value of the electric field at the center of the sphere for the case of plane wave incidence as shown in Figure 5(a) was computed by using the Mie Series [23] after scaling the ϵ_r of the sphere with frequency, as described earlier for the case of the slab, at a number of evenly spaced discrete frequencies, ranging from 50 Hz to 200 MHz. The value of the electric field at the scaled frequency was then scaled by the scale factor to obtain the actual value of the electric field at the frequency of interest, viz., $f = 50$ Hz. As shown in Figures 6(a) and 6(b) the amplitude and phase of the fields at 50 Hz remains nearly constant,

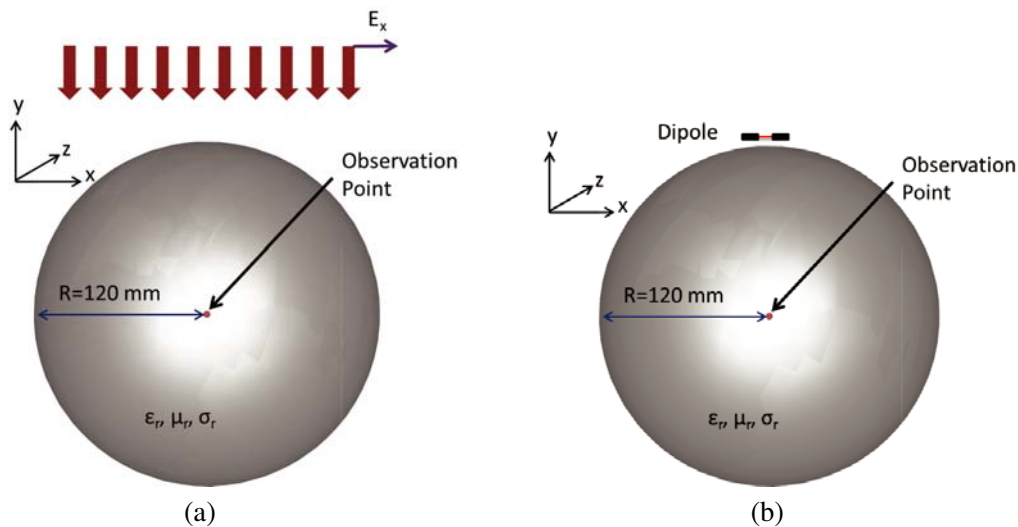


Figure 5. A sphere excited by x -polarized. (a) Plane wave, (b) short dipole.

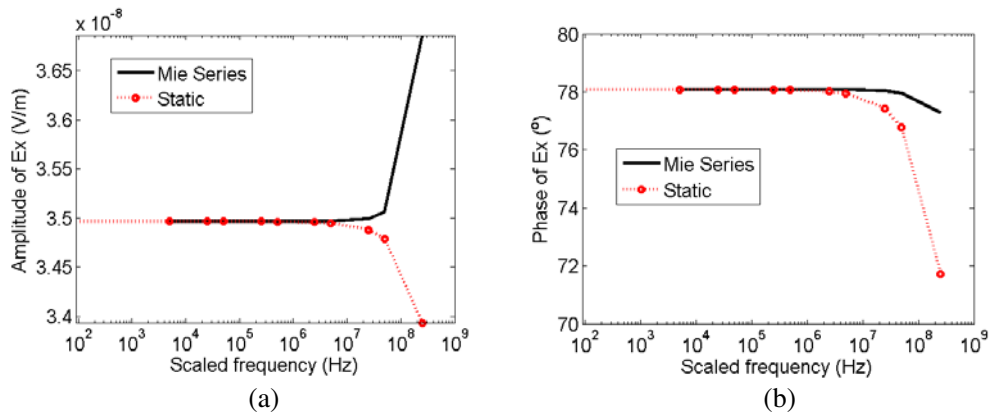


Figure 6. (a) Amplitude and (b) phase of E_x at the center of the sphere shown in Figure 5(a) for an x -polarized plane wave as a function of the solution frequency. (a) Amplitude of E_x , (b) phase of E_x .

Table 4. The value of the x -component of the electric field and y -component of magnetic field at the center of a sphere at 50 Hz due to an x -polarized plane wave incident on a sphere as shown in Figure 5(a).

Frequency (fs) (MHz)	Ex		Hy		Time Steps
	Amp (nV/m)	Phase (rad)	Amp (A/m)	Phase (rad)	
5	38	1.4	0.002666	3.1	22000
50	40	0.9	0.002745	2.6	2000

Table 5. The value of the x -component of the electric field and y -component of magnetic field at the center of a sphere at 50 Hz due to an x -polarized short dipole as shown in Figure 4(a).

Frequency (fs) (MHz)	Ex		Hy		Time Steps
	Amp (nV/m)	Phase (rad)	Amp (nA/m)	Phase (rad)	
5	185	-1.81	1.8	1.49	30000
50	198	-1.96	2	1.32	4000

irrespective of the frequency f_{sc} at which we solve the problem as long as the frequency is less than 60 MHz and also converges to the static field solution for a dielectric sphere [23]. These results have been further validated by using a numerical simulation using the FDTD, and the field values are given in Table 4. Also, we observe that for the case of plane-wave excitation of a sphere also, the values of the electric field at the scaled frequency needs to be scaled by the scale factor of ϵ_r to obtain the correct electric field at 50 Hz, but the value of magnetic field remains unchanged as we scale the ϵ_r , in common with the case of the slab. Also, the amplitudes and phases of the electric fields obtained from simulation are very close to the analytical Mie series solution in Figures 6(a) and 6(b).

This technique was also numerically validated for the case when an x -polarized short dipole source was used to excite the sphere as shown in Figure 5(b). The same approach of scaling the material parameters by the scale factor, followed by scaling the electric and magnetic fields by the same scale factor was applied to this case. Table 5 shows that the amplitude and phase of the electric and magnetic fields at the center of the sphere at 50 Hz remain unchanged as we scale the material parameters to two different scaled frequencies, i.e., 5 MHz and 500 kHz.

3.3. Application of the Proposed Solution to the Human Head Problem

The proposed scaling concept can be applied to the problem of modeling of brain waves inside the human head. To validate this technique for the case of the head problem the material parameters inside the human head at 50 Hz, given in Table 1, were scaled to 5 MHz and 50 MHz using Eq. (1). For some cases, such as the x -oriented dipole, it is possible to go down to even lower frequencies, namely, 100 kHz and 500 kHz to further test the scaling approach. Note that when the material parameters are scaled with frequency, the real parts of ϵ_r become much smaller than 1 (< 0.01), for some of the materials as seen from Table 1, though the imaginary parts of ϵ_r for these materials are much larger than real parts. Therefore, in order to mitigate the convergence problems, which arise when we try to model such low values of ϵ_r while using a dispersive model, we choose the real parts of ϵ_r for these materials to be unity and leave the conductivity unchanged. This is a valid approximation since the real parts of ϵ_r for these materials are much smaller than the equivalent imaginary part which is associated with the conductivity.

We have determined that the values of the fields at the same point located inside the head for three different orientations and locations of the short dipole on the surface of the head as shown in Figures 2(a), 2(b) and 2(c), by using two frequency-scaled models of the head, at 5 MHz and 50 MHz, respectively, are nearly same. The results are presented in Table 6. Table 7 shows that for the x -

Table 6. The value of the corresponding electric field component due to three different locations and polarizations of a dipole as shown in Figure 2 on the surface of the head at a point inside the human head at 50 Hz.

Frequency (fs) (MHz)	Amp. of Ex at Position 1 (nV/m)	Amp. of Ey at Position 2 (nV/m)	Amp. of Ez at Position 3 (nV/m)
5	170	900	550
50	170	780	480

Table 7. The value of the electric field at two different observation points inside the head at 50 Hz obtained by solving the fields due to a x -polarized dipole placed on top of the head (see Figure 2(a)), using four different equivalent head models derived by scaling the material parameters to four different frequencies, i.e., 100 kHz, 500 kHz, 5 MHz and 50 MHz.

Frequency (fs) (MHz)	Point 1	Point 2	Time Steps
	Ex at 50 Hz (nV/m)	Ex at 50 Hz (nV/m)	(for convergence)
0.1	175.9	65.3	4300000
0.5	170.8	67.8	2000000
5	167.2	49.0	400000
50	163.9	49.2	100000

Table 8. The value of the x -component of the electric field and y -component of magnetic field at a point inside the human head at 50 Hz due to an x -polarized short dipole as shown in Figure 2 (Position 1).

Frequency (fs) (MHz)	Ex		Hy		Time Steps
	Amp (nV/m)	Phase (rad)	Amp (pA/m)	Phase (rad)	
5	167.2	-1.9	60.97	1.48	400000
50	163.9	-1.9	65.64	1.55	100000

polarized dipole placed on top of the head (see Figure 2(a)), the value of the electric field at two different observation points inside the head remains nearly constant for four different scaled frequencies, i.e., 100 kHz, 500 kHz, 5 MHz and 50 MHz, but the number of time steps required for convergence, and hence the solution time, is decreased by 40 times as we increase the scaled frequency from 100 kHz to 50 MHz. The slight difference in the results at 500 kHz and 100 kHz may be because of the fact that the ABCs are only partially effective at such low frequencies, since this difference is not observed in the analytical solution for a sphere obtained by using the Mie series, which is shown in Figures 6(a) and 6(b). We observe that scaling the material parameters of the head with frequency improves the rate of convergence of the solution, which is retrieved at the frequency of interest by using the same scale factor as that used to scale ϵ_r . Table 8 reports the amplitudes and phases of Ex and Hy at 50 Hz for a x -polarized dipole placed on the surface of the head at position 1, as shown in Figure 2(a). It proves that even for the complex case of the human head not only the amplitude of electric field but its phase, and also the amplitude and phase of the magnetic field, remain invariant as we scale the material parameters of the head to a higher frequency in order to render the problem solvable.

3.4. Numerical Validation of Reciprocity

Next, we numerically validate the satisfaction of the reciprocity principle for this problem, which forms the basis of our simulation strategy. According to this principle, if a source dipole is placed inside the head and a receive dipole is placed on the surface of the head, the voltage induced in the receive dipole

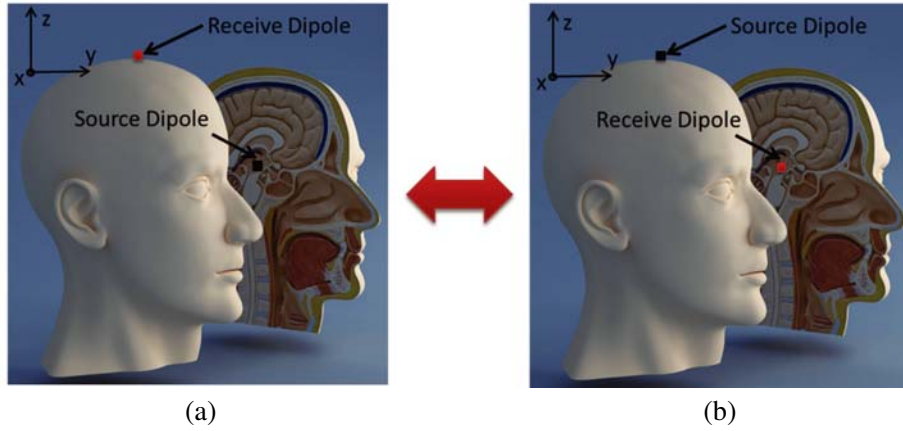


Figure 7. Reciprocity principle.

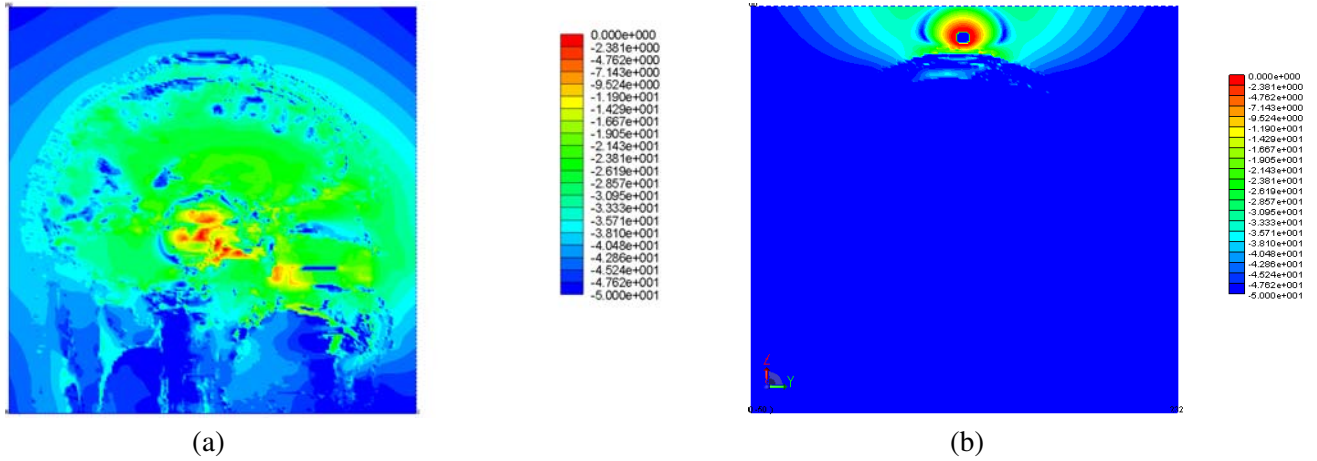


Figure 8. Amplitude of E_x (in dB) with the material parameters of the head scaled to 5 MHz from 50 Hz at 5 MHz due to (a) source dipole inside the head, (b) on the surface of the head. (a) Amplitude of E_x (in dB) due to a source dipole inside the head at 5 MHz, (b) amplitude of E_x (in dB) due to a source dipole on the surface of the head at 5 MHz.

would remain the same even when the position of the transmit and receive dipoles are interchanged. Figure 7 shows two x -polarized short dipoles, one inside the head and the other on the surface of the head. Figure 8 shows the field distribution in a plane perpendicular to x -axis and displaced by 20 mm in the x -direction from the center of an x -polarized dipole. Figure 8 confirms that as the dielectric constant of the material inside the head is very high, it acts as a cavity which does not allow most of the fields to escape when the source is placed inside the head, and does not allow the fields to enter the head when the source is placed outside the head. Figures 9(a) and 9(b) show the amplitude and the phase of the voltage received by the dipole inside at 5 MHz when the dipole outside is excited by using a Gaussian pulse. Figures 10(a) and 10(b) show the amplitude and the phase of voltage at 5 MHz when the source and receive dipoles are interchanged. As we can see from the two figures, the amplitude and phase of the induced voltage at 50 Hz is almost the same for the two cases, which verifies the numerical application of reciprocity principle.

All the numerical simulations were carried out by using a commercial FDTD code. The model of the head used in the code was discretized by using voxels each with a side 1 mm to accurately model the complex material distribution inside the head. Although the FDTD method was used in this paper, the proposed technique can also be used in conjunction with other numerical techniques such as the MoM and the FEM to solve low-frequency problems.

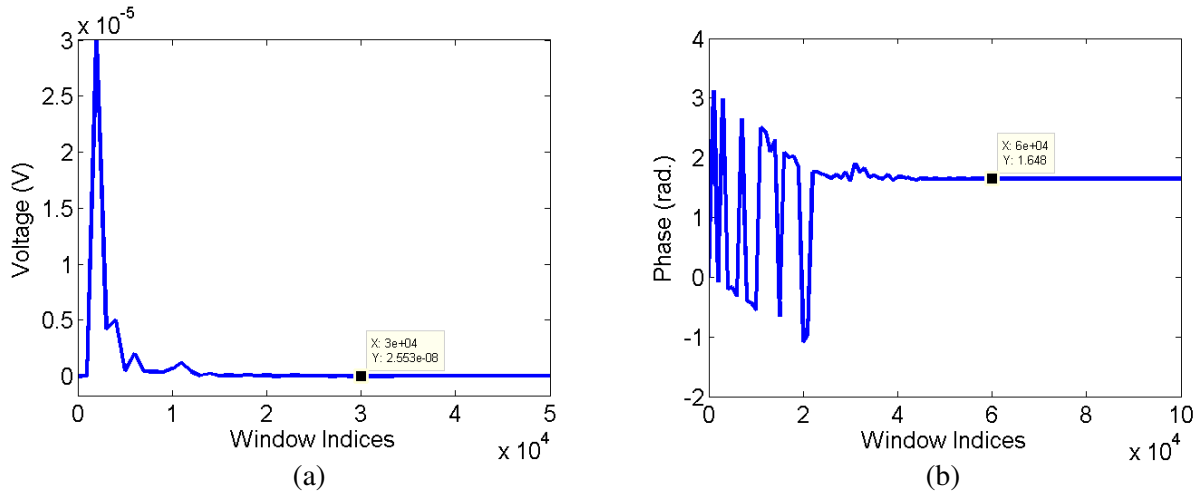


Figure 9. (a) Amplitude and (b) phase of voltage at the receive dipole located on the surface of the head due to a source dipole located inside the head as shown in Figure 7(a). (a) Amplitude of voltage as a function of number of time steps, (b) phase of voltage as a function of number of time steps.

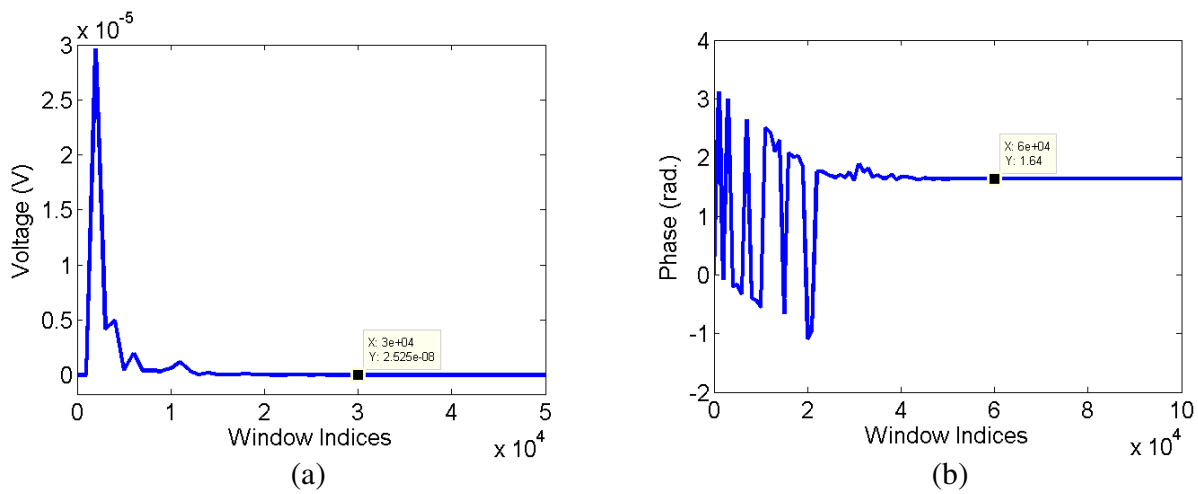


Figure 10. (a) Amplitude and (b) phase of voltage at the receive dipole located inside the head due to a source dipole on the surface of the head as shown in Figure 7(b). (a) Amplitude of voltage as a function of number of time steps, (b) phase of voltage as a function of number of time steps.

4. CONCLUSION

If we scale the ϵ_r with frequency and solve the problem at a higher frequency, the amplitude of electric field also gets scaled by a factor equal to the ratio of the scaled frequency and the problem frequency, while the phase remains nearly invariant. This hypothesis has been shown to be true for the case of a sphere by using the analytical Mie Series formulation and simulations. Also, the same technique has been validated for the case of full-wave modeling of brain waves inside the human head, with an estimated error of less than 10%. By solving the problem at a higher frequency after scaling the material parameters, the convergence rate of the solution can be increased significantly and the problem of increased reflections due to the ABCs at low frequencies can be overcome. This, in turn, facilitates the numerical modeling of the brain waves, which is a formidably challenging problem, owing to the low-frequency breakdown problem, which arises regardless of the numerical technique used.

REFERENCES

1. Suppes, P. and B. Han, "Brain-wave representation of words by superposition of a few sine waves," *Proc. Natl. Acad. Sci.*, Vol. 97, No. 15, 8738–8743, Jul. 18, 2000.
2. Pasley, B. N., S. V. David, N. Mesgarani, A. Flinker, S. A. Shamma, et al., "Reconstructing speech from human auditory cortex," *PLoS Biol.*, Vol. 10, No. 1, e1001251, 2012, doi: 10.1371/journal.pbio.1001251.
3. Hoole, P. R. P., K. Pirapaharan, S. A. Basar, R. Ismail, D. L. D. A. Liyanage, S. S. H. M. U. Senanayake, and S. R. H. Hoole, "Autism, EEG and brain electromagnetics research," *2012 IEEE EMBS Conference on Biomedical Engineering and Sciences (IECBES)*, 541–543, Dec. 17–19, 2012, doi: 10.1109/IECBES.2012.6498036.
4. Yasuhara, A., "Correlation between EEG abnormalities and symptoms of autism spectrum disorder (ASD)," *Brain and Development*, Vol. 32, No. 10, 791–798, Nov. 2010, ISSN 0387-7604, 10.1016/j.braindev.2010.08.010.
5. Fünfgeld, E. W., M. Baggen, P. Nedwidek, B. Richstein, and G. Mistlberger, "Double-blind study with phosphatidylserine (PS) in parkinsonian patients with senile dementia of Alzheimer's type (SDAT)," *Prog. Clin. Biol. Res.*, Vol. 317, 1235–1246, 1989.
6. Ponomareva, N. V., N. D. Selesneva, and G. A. Jarikov, "EEG alterations in subjects at high familial risk for Alzheimer's disease," *Neuropsychobiology*, Vol. 48, 152–159, 2003, doi: 10.1159/000073633.
7. NeuroSky Inc., "Brain wave signal (EEG) of NeuroSky, Inc.," Dec. 2009.
8. Yasui, Y., "A brainwave signal measurement and data processing technique for daily life applications," *J. Physiol. Anthropol.*, Vol. 28, No. 3, 145–150, 2009.
9. Fleur, K. L., K. Cassidy, A. Doud, K. Shades, E. Rogin, and B. He, "Quadcopter control in three-dimensional space using a noninvasive motor imagery-based brain-computer interface," *J. Neural. Eng.*, Vol. 10, 046003, Jun. 4, 2013, doi: 10.1088/1741-2560/10/4/046003.
10. Doud, A. J., J. P. Lucas, M. T. Pisansky, and B. He, "Continuous three-dimensional control of a virtual helicopter using a motor imagery based brain-computer interface," *PLoS ONE*, Vol. 6, e26322, 2011.
11. Galán, F., M. Nuttin, E. Lew, P. W. Ferrez, G. Vanacker, J. Philips, and R. del Millan, "A brain-actuated wheelchair: Asynchronous and non-invasive brain-computer interfaces for continuous control of robots," *Clin. Neurophysiol.*, 1192159–1192169, 2008.
12. Popescu, F., S. Fazli, Y. Badower, B. Blankertz, and K.-R. Müller, "Single trial classification of motor imagination using 6 dry EEG electrodes," *PLoS ONE*, Vol. 2, No. 7, e637, 2007, doi:10.1371/journal.pone.0000637.
13. Grozea, C., C. D. Voinescu, and S. Fazli, "Bristle-sensors — Low-cost flexible passive dry EEG electrodes for neurofeedback and BCI applications," *J. Neural. Eng.*, Vol. 8, 025008, 2011, doi:10.1088/1741-2560/8/2/025008.
14. Zhu, J. and D. Jiao, "A unified finite-element solution from zero frequency to microwave frequencies for full-wave modeling of large scale three-dimensional on-chip interconnect structures," *IEEE Trans. Adv. Packag.*, Vol. 31, No. 4, 873–881, Nov. 2008.
15. Gope, D., A. Ruehli, and V. Jandhyala, "Solving low-frequency EM-CKT problems using the PEEC method," *IEEE Trans. Adv. Packag.*, Vol. 30, No. 2, 313–320, May 2007.
16. Peratta, C. and A. Peratta, "Dielectric properties of biological tissues," *Topics in Engineering, Modelling the Human Body Exposure to ELF Electric Fields*, Vol. 47, 21–40, 2010.
17. Asami, K., "Dielectric properties of biological tissues in which cells are connected by communicating junctions," *Journal of Physics D — Applied Physics*, Vol. 40, No. 12, 3718–3727, Jun. 21, 2007, doi: 10.1088/0022-3727/40/12/027.
18. Kuang, W. and S. O. Nelson, "Low-frequency dielectric properties of biological tissues: A review with some new insights," *IEEE Transactions of the ASAE*, Vol. 41, No. 1, 173–184, Jan.–Feb. 1998.
19. Gabriel, C., S. Gabriel, and E. Corthout, "The dielectric properties of biological tissues. 1. Literature survey," *Physics in Medicine and Biology*, Vol. 41, No. 11, 2231–2249, Nov. 1996, doi:

- 10.1088/0031-9155/41/11/001.
20. Gabriel, S., R. W. Lau, and C. Gabriel, "The dielectric properties of biological tissues. 2. Measurements in the frequency range 10 Hz to 20 GHz," *Physics in Medicine and Biology*, Vol. 41, No. 11, 2251–2269, Nov. 1996, doi: 10.1088/0031-9155/41/11/002.
 21. Gabriel, S., R. W. Lau, and C. Gabriel, "The dielectric properties of biological tissues. 3. Parametric models for the dielectric spectrum of tissues," *Physics in Medicine and Biology*, Vol. 41, No. 11, 2271–2293, Nov. 1996, doi: 10.1088/0031-9155/41/11/003.
 22. Bossetti, C. A., M. J. Birdno, and W. M. Grill, "Analysis of the quasi-static approximation for calculating potentials generated by neural stimulation," *Journal of Neural Engineering*, Vol. 5, No. 1, 44–53, Mar. 2008, doi: 10.1088/1741-2560/5/1/005.
 23. Bohren, C. F. and D. R. Huffman, *Absorption and Scattering of Light by Small Particles*, Wiley-VCH, 82–101, Mar. 1998.